ADVANCED FUNCTIONAL MATERIALS
www.afm-journal.de

Oxygen Stoichiometry Effect on Polar Properties of $LaAlO_3$/$SrTiO_3$

Pankaj Sharma, Zhen Huang, Mengsha Li, Changjian Li, Songbai Hu, Hyungwoo Lee, Jung-Woo Lee, Chang-Beom Eom, Stephen J. Pennycook, Jan Seidel, Ariando, and Alexei Gruverman**

Discovery of a ferroelectric-like behavior of the $LaAlO_3$/$SrTiO_3$ (LAO/STO) interfaces provides an attractive platform for the development of nanoelectronic devices with functionality that can be tuned by electrical or mechanical means. However, further progress in this direction critically depends on deeper understanding of the physicochemical mechanism of this phenomenon. In this report, this problem by testing the electronic properties of the LAO/STO heterostructures with oxygen stoichiometry used as a variable is addressed. Local probe measurements in conjunction with interface electrical characterization allow to establish the field-driven reversible migration of oxygen vacancies as the origin of the ferroelectric-like behavior in LAO/STO. In addition, it is shown that oxygen deficiency gives rise to the formation of micrometer-long atomically sharp boundaries with robust piezoelectricity stemming from a significant strain gradient across the boundary region. These boundaries are not ferroelectric but they can modulate the local electronic characteristics at the interface. The obtained results open a possibility to design and engineer electromechanical functionality in a wide variety of nominally nonpolar and non-piezoelectric complex oxide heterostructures and thin films.

1. Introduction

Complex oxide heterointerfaces/heterostructures host plethora of intriguing physical phenomena, which do not exist in the constituent materials. The discovery of a high-mobility 2D electron gas (2DEG) at the $LaAlO_3$/$SrTiO_3$ (LAO/STO) interface is a prime example of such behavior.[1] Several mechanisms were proposed to explain its origin with no definitive consensus to date.[2–4] Irrespective of the origin, electronic confinement over a 2D plane along with a wide variety of approaches to tune the local electronic density, for example, via epitaxial strain,[5] atomic substitutions,[6] field effect,[7,8] and local charge writing,[9–11] offers a viable platform toward realization of advanced nanoelectronic devices.[12–14] The recently reported ferroelectric-like behavior of the LAO/STO heterostructures[15–17] provides for an alternative tuning mechanism for their electronic properties. The ferroelectric-like[18] behavior in LAO/STO, which manifests itself in an electrically induced switchable polarization, can be used not only to effectively gate the 2DEG at the heterointerface much like in the ferroelectric field effect transistors but also to nondestructively visualize the electrically controlled metal–insulator transitions at the nanoscale.[17,19] In addition, mechanical control of the induced polarization in the LAO/STO heterostructures presents a new paradigm for voltage-free tuning of 2DEG.[20] Despite these exciting developments, the fundamental mechanism of this phenomenon remains unclear.

In one of the earliest attempts to address this problem, it has been established experimentally that the switchable ferroelectric-like behavior of the LAO/STO thin film heterostructures arises from the LAO overlayer.[15] Theoretical

Dr. P. Sharma, S. Hu, Prof. J. Seidel
School of Materials Science and Engineering
UNSW Australia
Sydney, NSW 2052, Australia
E-mail: pankaj.sharma@unsw.edu.au
Dr. Z. Huang, Prof. Ariando
NUSNNI-NanoCore
National University of Singapore
117411, Singapore
Dr. Z. Huang, Prof. Ariando
Department of Physics
National University of Singapore
117542, Singapore
The ORCID identification number(s) for the author(s) of this article can be found under https://doi.org/10.1002/adfm.201707159.
M. S. Li, Dr. C. J. Li, Prof. S. J. Pennycook
Department of Materials Science and Engineering
National University of Singapore
117575, Singapore
Dr. H. Lee, J.-W. Lee, Prof. C.-B. Eom
Department of Materials Science and Engineering
University of Wisconsin
Madison, WI 53706, USA
Prof. A. Gruverman
Department of Physics and Astronomy and Nebraska Center for Materials and Nanoscience
University of Nebraska
Lincoln, NE 68588, USA
E-mail: alexei_gruverman@unl.edu

DOI: 10.1002/adfm.201707159

modeling predicted appearance of an intrinsic ferroelectric state in the biaxially strained LAO thin films at a compressive strain of more than 3%, due to freezing of the octahedral rotations.[21] However, the incipient ferroelectric state is usually suppressed by the dominant antiferrodistortive rotational modes. In addition, given that the LAO thin films in the LAO/STO heterostructures are under tensile strain (≈3%),[5] ruling out intrinsic ferroelectricity of the LAO thin films. Furthermore, the observed relaxation of electrically induced polarization states is reminiscent of the electret behavior, where polarization is induced by extrinsic mechanisms, such as transient separation of ionic charges/charged defects rather than by a stable long-range dipolar ordering.[22] Several surface charging mechanisms (related to the surface electrochemical processes or direct charge deposition via a biased probe), which could account for the observed ferroelectric-like behavior of the LAO/STO heterostructures, have been also proposed.[16,23,24] However, these surface-related mechanisms were challenged on the basis of observation of the switchable hysteretic response in the metal-gated LAO/STO heterostructures,[15,25] where the effects of surface charging can be largely ignored. The electrostatic force microscopy and piezoresponse force microscopy (EFM and PFM) measurements performed sequentially showed that the charges detected in the EFM and PFM modes were unrelated[15] suggesting a contribution of the bulk effects to the observed ferroelectric-like behavior. Later, a mechanism based upon a field-induced reversible migration of oxygen vacancies was put forward to explain the origin of the ferroelectric-like behavior of the LAO/STO heterostructures.[15,24] Plausibility of the proposed mechanism was evaluated using a field-time dependency of the locally written domains, which revealed a behavior consistent with a model based on field-assisted ion dynamics.[26] However, direct experimental proof of the proposed mechanism was still lacking.

In this work, we validate the field-induced oxygen vacancy migration as the root cause of the switchable ferroelectric-like behavior in the crystalline LAO/STO heterostructures by employing a set of LAO/STO samples with variable oxygen stoichiometry. Remarkably, varying oxygen stoichiometry also allowed observation of micrometer-long atomically sharp boundaries with robust piezoelectric activity in the oxygen-deficient LAO/STO heterostructures. These polar boundaries are not twin-walls commonly observed in ferroelastic materials, such as LAO,[27] but arise due to dislocations extending across the LAO/STO interface. Besides, it has been found that they affect the electronic characteristics of the 2DEG.

2. Results and Discussion

For this study, single crystalline epitaxial LAO films with the thickness of 25 unit cells on TiO_2-terminated (001) STO substrates were prepared using pulsed laser deposition equipped with in situ reflection high-energy electron diffraction (RHEED) under varying oxygen pressure (P_{O_2}) in the range of 10^{-3} to 10^{-5} Torr (see further details in Section S1, Supporting Information). **Figure 1**a shows a reciprocal space map around $(\bar{1}03)$ reflection, which suggests a coherent growth given that the in-plane lattice constant of 3.905 Å of the LAO thin film is same as of the underlying TiO_2-terminated STO substrate. Surface morphology of LAO/STO heterostructures display atomically flat step-terrace topology (Figure 1b) in agreement with the layer-by-layer growth mechanism inferred from the in situ RHEED oscillations during growth (Figure S1, Supporting Information). The interfacial electrical properties of the LAO/STO heterostructures were characterized using four-point Van der Pauw configuration. The observed interfacial sheet resistance as a function of temperature and oxygen pressure is summarized in Figure 1c. It can be seen

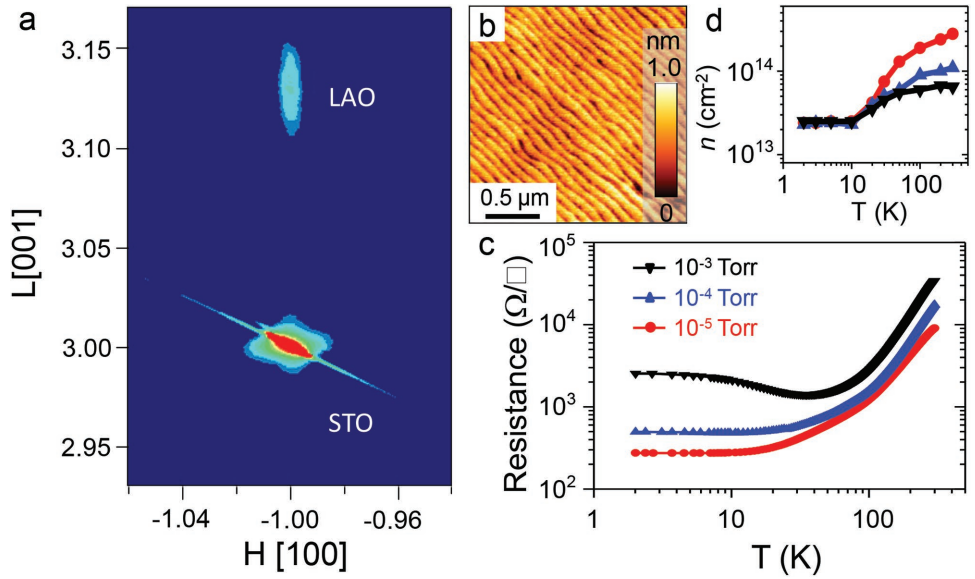

Figure 1. Structural and interface characterization. a) Reciprocal space map around $(\bar{1}03)$ peak for the LAO/STO heterostructure grown at $P_{O_2} = 10^{-3}$ Torr. b) Topographic image of the LAO/STO sample grown at $P_{O_2} = 10^{-3}$ Torr. c) Sheet resistance, and d) carrier density of the 2DEG at the interface of LAO/STO heterostructures grown at various partial pressures of the oxygen versus temperature.

that the interfacial sheet resistance decreases with decreasing temperature and with oxygen partial pressure during growth—a behavior consistent with the previously published data.[28–30] For temperatures ≤ 10 K, the sheet resistance saturates and shows an order of magnitude difference in the investigated oxygen pressure range of 10^{-3}–10^{-5} Torr. The decrease in the interfacial resistance with decreasing oxygen pressure is due to an increase in the oxygen vacancies concentration causing an increase in the electronic carrier density (from 6.4×10^{13} to 2.7×10^{14} cm^{-3} at 300 K, Figure 1d) and mobility. The observed change in the sheet resistance of the 2DEG at the LAO/STO interface in the investigated pressure range is still relatively small compared to heterostructures prepared under even stronger reducing conditions (i.e., 10^{-6} Torr), where oxygen vacancies-induced carriers start to dominate the interfacial conduction.[28] Nonetheless, in our case, LAO/STO interfaces prepared under various oxidation conditions show electrical characteristics consistent with the varying content of the oxygen vacancies. We note that the increase in the sheet resistance at low temperature for the sample grown under 10^{-3} Torr is likely due to the Kondo effect where mobile electrons are scattered by the magnetic centers.[28] A rough estimate of the density of the oxygen vacancies in the samples can be made based on temperature dependence of the measured interface electronic carrier density (Figure 1d). At 300 K, the net carrier density (n) at the interface consists of the contributions from both the oxygen vacancies (n_o) as well as polar-discontinuity-induced carriers (n_p).[31] At low temperature (2–3 K), only n_p is maintained and the oxygen vacancies-induced electrons contribution is "frozen-out."[31] Under the assumption that each oxygen vacancy (O_v) provides two mobile electrons at 300 K, the O_v density can be calculated as: 0.5*[n(300 K)–n(2 K)], where n(300 K) and n(2 K) is the measured net carrier density at 300 and 2 K, respectively. These values can readily be obtained from Figure 1d. Using this equation, the estimated O_v densities for different samples are as follows: for the sample grown at P_{O_2} of 10^{-3} Torr, the O_v density is 2×10^{13} cm^{-2}; for the sample grown at P_{O_2} of 10^{-4} Torr, it is 4.4×10^{13} cm^{-2} and for the sample grown at P_{O_2} of 10^{-5} Torr, the O_v density is 12.8×10^{13} cm^{-2}.

The effect of oxygen stoichiometry on the electrically induced ferroelectric-like behavior of the LAO/STO heterostructures was probed by a combined use of PFM and EFM (details in Supporting Information).[15,16,20,24,26,32] A bidomain pattern consisting of square-shaped concentric domains was produced by scanning the sample surface with an atomic force microscopy (AFM) tip under ±5 V DC bias. The PFM and EFM images were acquired to test the bias-induced electromechanical behavior and surface electrical charges, respectively in the samples grown under different oxygen pressure P_{O_2} (**Figure 2**). For the LAO/STO heterostructure grown at the highest used P_{O_2} of 10^{-3} Torr, the PFM signal is unstable and is dominated by the electrostatic response (Figure 2a,b).[15] This conclusion is based on the fact that the PFM amplitude image exhibits a uniform low response over the entire outer square frame and just a small phase change (much less than 180°) is seen in the PFM phase image. On the other hand, the EFM image (Figure 2c) reveals deposition of surface charges, which is illustrated by opposite EFM contrast of the regions produced by scanning with the tip bias of opposite polarity and is in agreement with the previously reported results.[15,26]

PFM/EFM testing of the oxygen deficient LAO/STO heterostructures reveals a completely different behavior (Figure 2d–i). In this case, a clear ferroelectric-like behavior can be observed—stable PFM phase contrast for oppositely poled regions (Figure 2e,h), which appear as areas of the same intensity separated by the dark lines (domain walls) in the PFM amplitude image (Figure 2d,g). These characteristics, which illustrate a strong electromechanical response due to the electrically induced polarization, become particularly evident for the lowest used oxygen pressure 10^{-5} Torr. Note that although EFM of the samples grown at 10^{-4} and 10^{-5} Torr still shows the presence of the surface charges deposited as a result of poling (Figure 2f,i), the relative contribution of the electrostatic signal to the total measured PFM signal is significantly smaller than for the samples grown at 10^{-3} Torr.

To gain further insight into the electrically induced switchable polarization behavior, local spectroscopic piezoresponse hysteresis measurements were performed (**Figure 3**). While the LAO/STO samples grown at $P_{O_2} = 10^{-3}$ Torr did not show any switchable behavior (Figure 3a,b), the samples grown at lower oxygen pressures revealed a distinct switching behavior typical for classical ferroelectric materials, such as $Pb(Zr_xTi_{1-x})O_3$ and $BaTiO_3$ (Figure 3c–f). At coercive biases, the inversion of the electrically induced polarization is highlighted by a phase change of ≈180° in the PFM phase loops. This transition becomes sharper with the P_{O_2} decrease (Figure 3c,e). Also, from the PFM amplitude hysteresis loops, the initial piezoresponse (i.e., piezoresponse at 0 DC bias, which is a measure of the as-grown polarization) increases with the P_{O_2} decrease in agreement with the data in Figure 2.

The obtained results provide solid experimental evidence for the role of the oxygen vacancies in the electrically induced ferroelectric-like switching behavior and interface conductivity of the LAO/STO heterostructures, which was hypothesized in our earlier studies.[15,20] Also, for the LAO/STO thin film heterostructures grown on the LAO substrate, similar dependency of the ferroelectric-like behavior on the growth pressure of the oxygen was observed (Figure S3, Supporting Information). An increased concentration of oxygen vacancies in the LAO/STO samples grown at relatively low oxygen pressure (i.e., 10^{-5} Torr) under an electrical bias leads to the formation of switchable polarization states due to the field-induced redistribution of oxygen vacancies. Additionally, increasing concentration of oxygen vacancies leads to an enhanced electron density at the interface, thereby decreasing the interface sheet resistance (Figure S2, Supporting Information).[15,19] However, we note that the interfacial charge cannot be a reason for the observed ferroelectric-like behavior. This mechanism can be ruled out based on the fact that the similar behavior has also been observed in epitaxial single-crystalline as well as amorphous $LaAlO_3$ thin films (in the absence of the STO layer)[26,33] with no 2DEG at the interface. Similarly, rise of intrinsic ferroelectricity is unlikely since the observed field-time dependence of the locally written domains exhibits a much slower switching than is typically seen in the ferroelectric films suggesting an ion-mediated mechanism.[16,26]

Close examination of the oxygen-deficient LAO/STO heterostructures (specifically, those grown at 10^{-5} Torr) reveals structural features appearing as micrometer-long unit-cell-high nanometer-wide lines typically running in the directions parallel or perpendicular to the terrace step edges (**Figure 4**a,d;

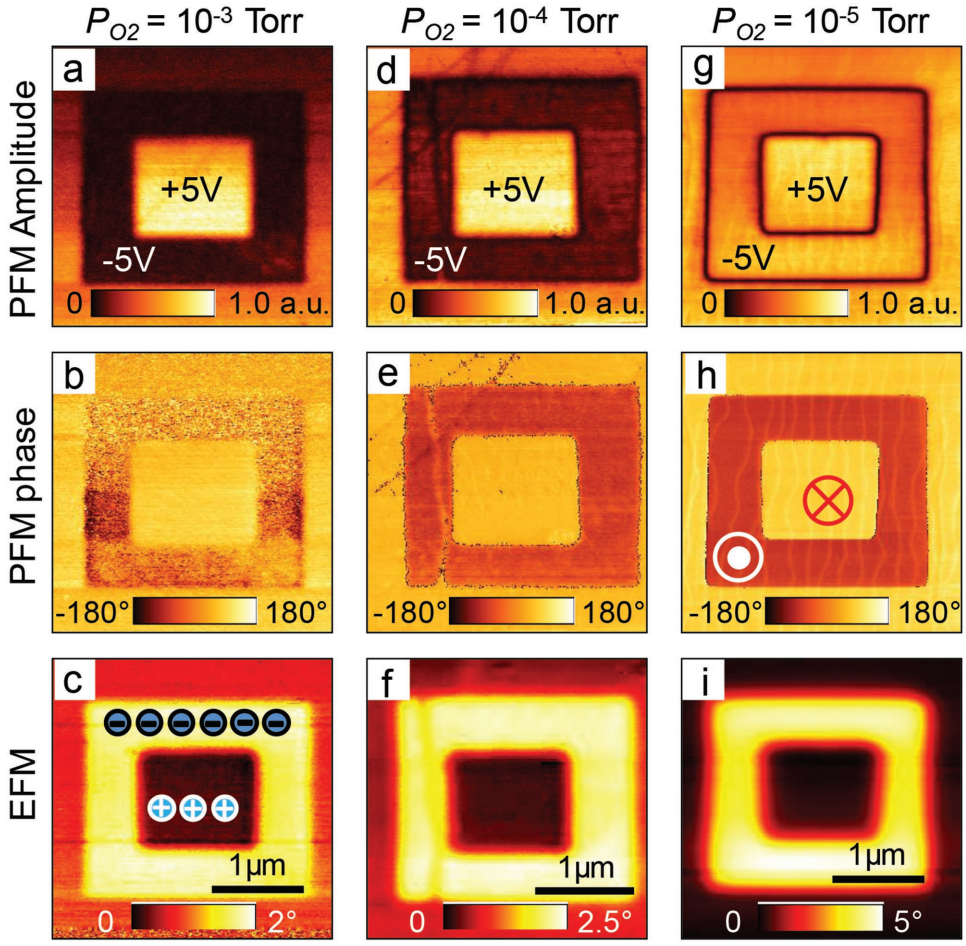

Figure 2. Effect of oxygen-stoichiometry on ferroelectric-like behavior. a–i) PFM amplitude (a,d,g), PFM phase (b,e,h), and the corresponding EFM (c,f,i) images of the poled regions generated in the LAO/STO heterostructures grown at different partial oxygen pressures (P_{O_2}). Images of the LAO/STO heterostructures grown at P_{O_2} = 10^{-3}, 10^{-4}, and 10^{-5} Torr are shown in the 1st column (a–c), 2nd column (d–f), and 3rd column (g–i), respectively. EFM phase images are acquired at a DC read bias of +3 V.

Figure S4, Supporting Information). It could be assumed that these lines represented interfaces associated either with the twin boundaries, which commonly arise in ferroelastic materials such as $LaAlO_3$,[34–36] or structural distortions that extend across the LAO/STO interface.[37] However, based on their morphological images, the observed structures do not exhibit the characteristics typical for the ferroelastic twin boundaries, which always run along the well-defined crystallographic directions, and are absolutely straight unless they intersect or impinge upon each other, as for example, in the case of a tweed structure.[27,36] The observed features also appear to stick out from the surface like nanowires in contrast to the twin boundaries. Further, in thin films, the ferroelastic twins tend to appear in the form of tweed structure—dense self-ordered arrays with domain size comparable to the film thickness.[38] Thus, the lines observed in Figure 4 cannot be interpreted as ferroelastic twin boundaries.

Next, to test the properties of the observed boundaries, high-resolution PFM imaging was performed in their pristine state (i.e., without any previous poling of the sample) (Figure 4b,c). It can be seen that the boundaries exhibit a strongly enhanced PFM signal: in comparison with the background signal from the crystalline matrix their PFM amplitude signal is nearly twice as large. The width of the boundaries determined from the AFM topographic image, is found to be ≈30 nm. However, the corresponding piezoresponse peak is much wider, i.e., ≈160 nm suggesting that a strain coupled to the local dipole is gradually changing across the boundaries. The switchability of these boundaries was investigated by writing and imaging concentric square domains of opposite polarity (Figure 4(d–f). It can be seen that the piezoresponse signal along the boundaries remained unperturbed. Specifically, the PFM phase does not change its sign upon application of a DC bias and the PFM amplitude signal is not altered either, which means that polarity cannot be switched or erased (Figure 4e,f). Thus, the boundaries display piezoelectricity, however, they are not ferroelectric. All scanning probe microscopy measurements were performed at room temperature (≈300 K) under ambient conditions (further details can be found in Section S2, Supporting Information).

To examine the origin and characteristics of the boundaries, high-resolution XRD scans were recorded around (002)

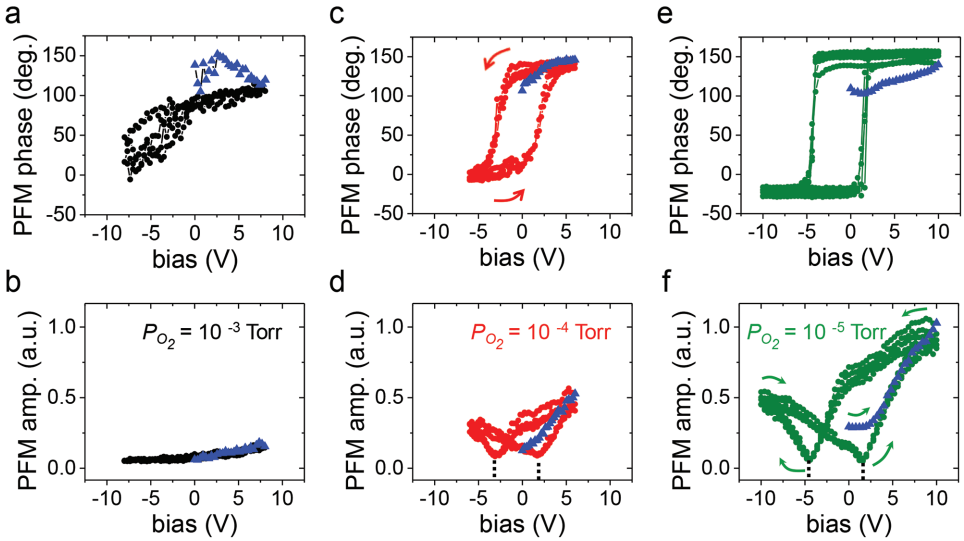

Figure 3. Effect of oxygen-stoichiometry on local piezoresponse hysteresis loops. (a–f) Local spectroscopic PFM phase (a,c,e) and amplitude (b,d,f) response versus DC bias acquired on LAO/STO heterostructures grown at different partial pressures of the oxygen (P_{O_2}). Spectroscopic curves measured on LAO/STO heterostructures grown at $P_{O_2} = 10^{-3}$, 10^{-4}, and 10^{-5} Torr are shown in 1st column (a,b), 2nd column (c,d), and 3rd column (e,f), respectively. For all the loops, the initial quarter cycle is shown in the blue color.

reflections. The θ–2θ scan (**Figure 5**a) shows clear thickness fringes (estimated thickness of about ≈10 nm) in the sample grown at $P_{O_2} = 10^{-5}$ Torr illustrating its high structural quality. Further, the rocking curve scan (Figure 5b) shows diffuse shoulders on either side of the LAO (002) reflection in contrast to the sample LAO/STO prepared at high oxygen pressure. However, the intensity of shoulder peaks is very weak, indicating the formation of local domain structure (probably without the long-range periodicity) in the LAO layer.[37,39] To gain further insight, high-resolution, aberration-corrected, high-angle annular dark field (HAADF) scanning transmission electron microscopy (STEM) imaging was performed (details in Supporting Information). Atomically resolved STEM imaging reveals a low angle grain boundary to be present in the LAO (shown by an

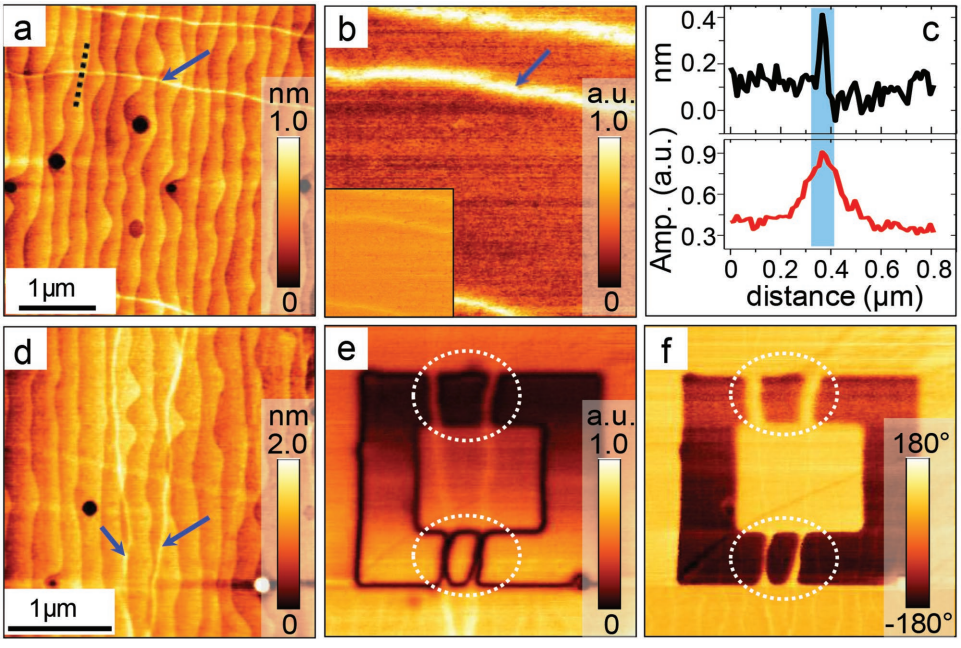

Figure 4. Enhanced piezoelectricity at structural boundaries in LAO/STO sample grown at oxygen pressure of 10^{-5} Torr. a) Topography and b) the corresponding PFM amplitude image of the pristine LAO/STO sample. Inset in (b) shows simultaneously acquired PFM phase image. c) Cross-section analysis of the images (a,b) along the dotted black line shown in (a). Piezoresponse after electrical poling (d–f): topography (d), PFM amplitude (e), and the corresponding PFM phase image (f) acquired after electrical poling of the concentric square-frames. Electrical poling by a DC bias of –5 V for the outer box, while with +5 V for the inner square box.

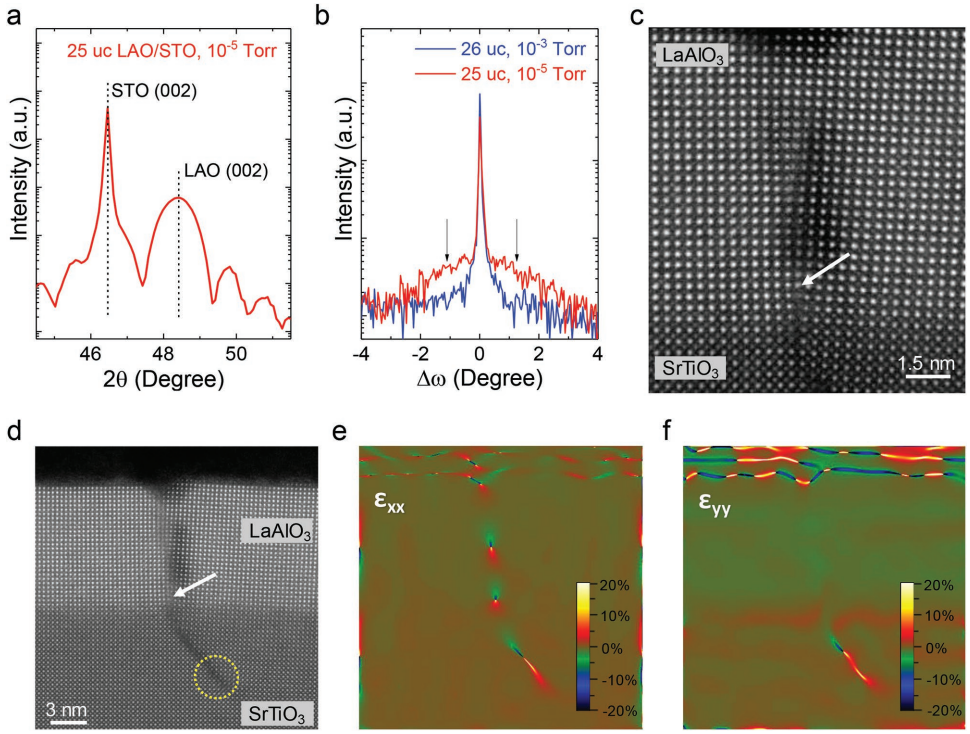

Figure 5. High-resolution X-ray diffraction and scanning transmission electron microscopy (STEM). a) A high-resolution θ–2θ scan around the LAO (002) diffraction peak for LAO/STO sample grown at $P_{O_2} = 10^{-5}$ Torr. b) A rocking-curve scan around the LAO (002) diffraction peak for LAO/STO samples grown at $P_{O_2} = 10^{-3}$ Torr and 10^{-5} Torr. c) A representative high-resolution HAADF–STEM image of an isolated boundary viewed along the [010] direction in the 10^{-5} Torr LAO/STO sample. d) HAADF–STEM image of an isolated boundary, and e) corresponding maps of strain distribution in the in-plane ε_{xx} and f) out-of-plane ε_{yy} directions, respectively.

arrow in Figure 5c). This boundary originates as a result of a structural distortion (i.e., dislocation, shown by the dotted yellow circle in Figure 5d) in the STO that couples across the interface. This type of structural distortion could be the origin of the piezoelectrically active boundaries seen in Figure 4. Geometric phase analysis quantifies the strain distribution across these boundaries (Figure 5e,f).[40,41] As can be seen, a significant strain gradient exists both in the in-plane (ε_{xx}) and out-of-plane (ε_{yy}) directions across the boundary region, which explains the observed high piezoresponse signal at such boundaries. An obvious discrepancy between the width of the dislocation as seen in the STEM image in Figure 5c, which is in the range of several unit cells, and the width of the boundaries determined by AFM in Figure 4a,c can be due to convolution effect of the probing tip (typical apex curvature radius is ≈30 nm) and surface topographical features. The structural distortions at the boundaries are frozen in space, and therefore the observed piezoresponse is not switchable upon application of an electric field. Nonetheless, the built-in polarity at the boundaries could likely control the local 2DEG properties at the interface.

To elucidate polarity-2DEG correlation, combined PFM, EFM, and scanning Kelvin probe microscopy (SKPM) measurements were performed in the LAO/STO samples grown at oxygen pressure of 10^{-5} Torr (**Figure 6**). As before, PFM measurements detect a high electromechanical response, whereas EFM reveals a decreased phase shift over the boundaries (Figure 6a–c). The decreased EFM phase shift is consistent with a greater accumulation of the positively charged oxygen vacancies in the vicinity of the observed boundaries in the bulk of the LAO thin film away from the sample surface.[15] Thus, an enhanced concentration of the electrons at the LAO/STO interface around the structural boundaries is expected.[15,20,24] The SKPM measurements over the same area show an increase in the surface potential by ≈50–60 mV signifying a change in the local electronic band structure (Figure 6d,e). The surface potential increase indicates a localized decrease in the work function of LAO/STO heterostructures and is consistent with an enhanced local density of electrons at the interface. Another mechanism, such as exchange of cations near the interface at the boundaries, could be an additional factor influencing the electronic density at the interface. However, such a high-resolution elemental investigation is outside the scope of the present work.

These results are of significance in light of recent experimental demonstration of the existence of polar tweeds in mechanically stressed $LaAlO_3$ single crystal.[27] Even though the observed boundaries in our case are not twin walls they do display similar polar characteristics. Their polar behavior can be attributed to the large strain gradients across the structural distortions (dislocations) that proliferate across the LAO/STO interface and give rise to the appearance of these boundaries. Since these features are not observed in the LAO/STO heterostructures grown at high partial oxygen pressure, it is reasonable to assume that oxygen vacancies play an important role in the piezoelectric behavior of these boundaries through the suppression of primary antiferrodistortive distortions (described as oxygen-octahedra

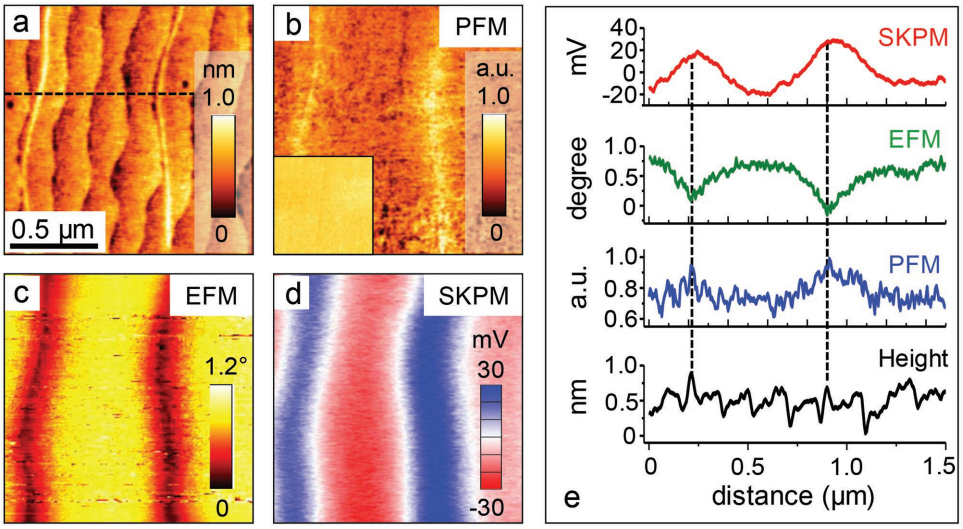

Figure 6. Electronic/electrical characteristics at the boundaries in the LAO/STO sample grown at oxygen pressure of 10^{-5} Torr. a) Topography, b) PFM amplitude, c) EFM, and d) the corresponding SKPM image acquired around structural boundaries/twin-walls of the LAO/STO heterostructures. Inset in (b) shows simultaneously acquired PFM phase image. e) Cross-section analysis of the images (a–d) along the dotted black line shown in (a). EFM phase image in (c) is acquired at a DC read bias of +2 V.

tiltings and rotations).[36] Moreover, if the STO had pre-existing cracks then oxygen stoichiometry should not play a significant role (also to note STO substrates used were of same type and were treated similarly before growth). This is contrary to the experimental observation. Therefore, we believe that the cracks appear due to growth conditions likely because of the interplay between oxygen stoichiometry and local strain relaxation.[42–44] As a final note, we would also like to point out that there is no appreciable off-centering of the Al cations within the LAO unit cell suggesting that inversion symmetry is not broken (for details, see Section S6, Figure S5, Supporting Information).

3. Conclusion

In summary, the LAO/STO thin film heterostructures with varying oxygen stoichiometry have been fabricated and investigated to unveil the mechanism of the ferroelectric-like behavior of LAO/STO. The experimental approach is based on using a combination of complimentary scanning probe microscopy techniques with electrical characterization of the 2DEG at the LAO/STO interface. The obtained results unambiguously confirm the hypothesized model based upon field-driven reversible migration of oxygen vacancies as the origin of the observed ferroelectric-like behavior in the LAO/STO thin film heterostructures. Another significant finding is oxygen stoichiometry controlled appearance of polar boundaries with strong piezoelectric response arising due to structural distortions, such as dislocations, that extend across the interface. Polarity of these structural boundaries is not switchable, which rules out the presence of intrinsic ferroelectricity. Nonetheless, the built-in polarity of the boundaries does affect the electronic characteristics of the heterostructures and may lead to an increased electronic density at the heterointerface. Given a continuously growing emphasis on device miniaturization, these polar boundaries present new possibilities for realization of advanced nanoscale device (provided a greater control over their density and spatial location will be achieved). Just to mention that the earlier notable examples of unexpected functionalities associated with the atomically sharp grain boundaries in insulating perovskites include piezoelectricity in nonpolar STO,[45] and electrically conductive hot-spots of nanoscale dimensions.[46] The obtained results provide an insight into the possible routes to design and engineer heterointerface functionalities not available in the constituent materials.

Supporting Information

Supporting Information is available from the Wiley Online Library or from the author.

Acknowledgements

P.S. and Z.H. contributed equally to this work. The work at the University of Nebraska was supported by the National Science Foundation (NSF) through Materials Research Science and Engineering Center (MRSEC) under Grant No. DMR-1420645. P.S. and J.S. acknowledge the funding supported by the Australian Research Council (ARC) through Discovery Grants. This research was supported in part by the Australian Research Council Centre of Excellence in Future Low-Energy Electronics Technologies (Project No. CE170100039) and funded by the Australian Government. The work at the University of Wisconsin was supported by AFOSR under Grant No. FA9550-15-1-0334.

Conflict of Interest

The authors declare no conflict of interest.

Keywords

complex oxide heterointerfaces, oxygen stoichiometry, polar boundaries, scanning probe microscopy

Received: December 8, 2017
Revised: March 3, 2018
Published online: April 23, 2018

[1] A. Ohtomo, H. Y. Hwang, *Nature* **2004**, *427*, 423.
[2] N. Nakagawa, H. Y. Hwang, D. A. Muller, *Nat. Mater.* **2006**, *5*, 204.
[3] G. Herranz, M. Basletić, M. Bibes, C. Carrétéro, E. Tafra, E. Jacquet, K. Bouzehouane, C. Deranlot, A. Hamzić, J.-M. Broto, A. Barthélémy, A. Fert, *Phys. Rev. Lett.* **2007**, *98*, 216803.
[4] P. R. Willmott, S. A. Pauli, R. Herger, C. M. Schlepütz, D. Martoccia, B. D. Patterson, B. Delley, R. Clarke, D. Kumah, C. Cionca, Y. Yacoby, *Phys. Rev. Lett.* **2007**, *99*, 155502.
[5] C. W. Bark, D. A. Felker, Y. Wang, Y. Zhang, H. W. Jang, C. M. Folkman, J. W. Park, S. H. Baek, H. Zhou, D. D. Fong, X. Q. Pan, E. Y. Tsymbal, M. S. Rzchowski, C. B. Eom, *Proc. Natl. Acad. Sci. USA* **2011**, *108*, 4720.
[6] H. W. Jang, D. A. Felker, C. W. Bark, Y. Wang, M. K. Niranjan, C. T. Nelson, Y. Zhang, D. Su, C. M. Folkman, S. H. Baek, S. Lee, K. Janicka, Y. Zhu, X. Q. Pan, D. D. Fong, E. Y. Tsymbal, M. S. Rzchowski, C. B. Eom, *Science* **2011**, *331*, 886.
[7] A. D. Caviglia, S. Gariglio, N. Reyren, D. Jaccard, T. Schneider, M. Gabay, S. Thiel, G. Hammerl, J. Mannhart, J.-M. Triscone, *Nature* **2008**, *456*, 624.
[8] C. Bell, S. Harashima, Y. Kozuka, M. Kim, B. G. Kim, Y. Hikita, H. Y. Hwang, *Phys. Rev. Lett.* **2009**, *103*, 226802.
[9] Y. Xie, C. Bell, T. Yajima, Y. Hikita, H. Y. Hwang, *Nano Lett.* **2010**, *10*, 2588.
[10] C. Cen, S. Thiel, G. Hammerl, C. W. Schneider, K. E. Andersen, C. S. Hellberg, J. Mannhart, J. Levy, *Nat. Mater.* **2008**, *7*, 298.
[11] Y. Xie, C. Bell, Y. Hikita, H. Y. Hwang, *Adv. Mater.* **2011**, *23*, 1744.
[12] C. Cen, S. Thiel, J. Mannhart, J. Levy, *Science* **2009**, *323*, 1026.
[13] P. Irvin, Y. Ma, D. F. Bogorin, C. Cen, C. W. Bark, C. M. Folkman, C.-B. Eom, J. Levy, *Nat. Photonics* **2010**, *4*, 849.
[14] G. L. Cheng, P. F. Siles, F. Bi, C. Cen, D. F. Bogorin, C. W. Bark, C. M. Folkman, J. W. Park, C. B. Eom, G. Medeiros-Ribeiro, J. Levy, *Nat. Nanotechnol.* **2011**, *6*, 343.
[15] C. W. Bark, P. Sharma, Y. Wang, S. H. Baek, S. Lee, S. Ryu, C. M. Folkman, T. R. Paudel, A. Kumar, S. V. Kalinin, A. Sokolov, E. Y. Tsymbal, M. S. Rzchowski, A. Gruverman, C. B. Eom, *Nano Lett.* **2012**, *12*, 1765.
[16] A. Kumar, T. M. Arruda, Y. Kim, I. N. Ivanov, S. Jesse, C. W. Bark, N. C. Bristowe, E. Artacho, P. B. Littlewood, C.-B. Eom, S. V. Kalinin, *ACS Nano* **2012**, *6*, 3841.
[17] M. Huang, F. Bi, C.-W. Bark, S. Ryu, K.-H. Cho, C.-B. Eom, J. Levy, *Appl. Phys. Lett.* **2014**, *104*, 161606.
[18] R. K. Vasudevan, N. Balke, P. Maksymovych, S. Jesse, S. V. Kalinin, *Appl. Phys. Rev.* **2017**, *4*, 021302.
[19] M. Huang, F. Bi, S. Ryu, C.-B. Eom, P. Irvin, J. Levy, *APL Mater.* **2013**, *1*, 052110.
[20] P. Sharma, S. Ryu, J. D. Burton, T. R. Paudel, C. W. Bark, Z. Huang, Ariando, E. Y. Tsymbal, G. Catalan, C. B. Eom, A. Gruverman, *Nano Lett.* **2015**, *15*, 3547.
[21] A. J. Hatt, N. A. Spaldin, *Phys. Rev. B* **2010**, *82*, 195402.
[22] M. E. Lines, A. M. Glass, *Principles and Applications of Ferroelectrics and Related Materials*, Oxford University Press, Oxford, UK **1977**.
[23] F. Bi, D. F. Bogorin, C. Cen, C. W. Bark, J.-W. Park, C.-B. Eom, J. Levy, *Appl. Phys. Lett.* **2010**, *97*, 173110.
[24] C. Li, Y. Cao, Y. Bai, A. Li, S. Zhang, D. Wu, *ACS Appl. Mater. Interfaces* **2015**, *7*, 10146.
[25] F. Bi, M. Huang, C.-W. Bark, S. Ryu, S. Lee, C.-B. Eom, P. Irvin, J. Levy, *J. Appl. Phys.* **2016**, *119*, 025309.
[26] P. Sharma, S. Ryu, Z. Viskadourakis, T. R. Paudel, H. Lee, C. Panagopoulos, E. Y. Tsymbal, C.-B. Eom, A. Gruverman, *Adv. Funct. Mater.* **2015**, *25*, 6538.
[27] E. K. H. Salje, M. Alexe, S. Kustov, M. C. Weber, J. Schiemer, G. F. Nataf, J. Kreisel, *Sci. Rep.* **2016**, *6*, 27193.
[28] A. Brinkman, M. Huijben, M. van Zalk, J. Huijben, U. Zeitler, J. C. Maan, W. G. van der Wiel, G. Rijnders, D. H. A. Blank, H. Hilgenkamp, *Nat. Mater.* **2007**, *6*, 493.
[29] A. Kalabukhov, R. Gunnarsson, J. Börjesson, E. Olsson, T. Claeson, D. Winkler, *Phys. Rev. B* **2007**, *75*, 121404(R).
[30] W. Siemons, G. Koster, H. Yamamoto, W. A. Harrison, G. Lucovsky, T. H. Geballe, D. H. A. Blank, M. R. Beasley, *Phys. Rev. Lett.* **2007**, *98*, 196802.
[31] Z. Q. Liu, C. J. Li, W. M. Lu, X. H. Huang, Z. Huang, S.W. Zeng, X. P. Qiu, L. S. Huang, A. Annadi, J. S. Chen, J. M. D. Coey, T. Venkatesan, Ariando, *Phys. Rev. X* **2013**, *3*, 021010.
[32] P. Sharma, J. Seidel, in *Advanced Materials Interfaces* (Eds: A. Tiwari, H. K. Patra, X. Wang), John Wiley & Sons, New York, USA **2016**.
[33] A. S. Borowiak, N. Baboux, D. Albertini, B. Vilquin, G. S. Girons, S. Pelloquin, B. Gautier, *Appl. Phys. Lett.* **2014**, *105*, 012906.
[34] R. J. Harrisona, E. K. H. Salje, *Appl. Phys. Lett.* **2010**, *97*, 021907.
[35] E. K. H. Salje, M. A. Carpenter, *Appl. Phys. Lett.* **2011**, *99*, 051907.
[36] E. K. H. Salje, *Am. Mineral.* **2015**, *100*, 343.
[37] J. E. Boschker, C. Folkman, C. W. Bark, Å. F. Monsen, E. Folven, J. K. Grepstad, E. Wahlström, C. B. Eom, T. Tybell, *Phys. Rev. B* **2011**, *84*, 205418.
[38] A. L. Roytburd, in *Thin Film Ferroelectric Materials and Devices* (Ed: R. Ramesh), Springer, Boston, MA **1997**, p. 71–90.
[39] V. M. Kaganer, R. Kohler, M. Schmidbauer, R. Opitz, B. Jenichen, *Phys. Rev. B* **1997**, *55*, 1793.
[40] M. J. Hÿtch, E. Snoeck, R. Kilaas, *Ultramicroscopy* **1998**, *74*, 131.
[41] K.-H. Kim, *Appl. Microsc.* **2015**, *45*, 101.
[42] D. Lee, A. Yoon, S. Y. Jang, J.-G. Yoon, J.-S. Chung, M. Kim, J. F. Scott, T. W. Noh, *Phys. Rev. Lett.* **2011**, *107*, 057602.
[43] D. Lee, T. W. Noh, *Philos. Trans. R. Soc., A* **2012**, *370*, 4944.
[44] Y. J. Shin, L. Wang, Y. Kim, H.-H. Nahm, D. Lee, J R. Kim, S. M. Yang, J.-G. Yoon, J-S. Chung, M. Kim, S. H. Chang, T. W. Noh, *ACS Appl. Mater. Interfaces* **2017**, *9*, 27305.
[45] J. Petzelt, T. Ostapchuk, I. Gregora, I. Rychetský, S. Hoffmann-Eifert, A. V. Pronin, Y. Yuzyuk, B. P. Gorshunov, S. Kamba, V. Bovtun, J. Pokorný, M. Savinov, V. Porokhonskyy, D. Rafaja, P. Vaněk, A. Almeida, M. R. Chaves, A. A. Volkov, M. Dressel, R. Waser, *Phys. Rev. B* **2001**, *64*, 184111.
[46] K. Szot, W. Speier, G. Bihlmayer, R. Waser, *Nat. Mater.* **2006**, *5*, 312.